INDIAN JOURNAL OF SCIENCE AND TECHNOLOGY

RESEARCH ARTICLE

OPEN ACCESS
Received: 14-06-2024
Accepted: 24-08-2024
Published: 08-10-2024

Citation: Dang K, Makkar V, Sharma N (2024) Radiative MHD Casson Non-Newtonian Nanofluid Slip Flow Induced by Stretching Cylinder: A Numerical Approach . Indian Journal of Science and Technology 17(38): 3993-4004. https://doi.org/10.17485/IJST/v17i38.1978

* **Corresponding authors**.
vini252011makkar@gmail.com
naresh.sharma2006@gmail.com

Funding: None

Competing Interests: None

Copyright: © 2024 Dang et al. This is an open access article distributed under the terms of the Creative Commons Attribution License, which permits unrestricted use, distribution, and reproduction in any medium, provided the original author and source are credited.

Published By Indian Society for Education and Environment (iSee)

ISSN
Print: 0974-6846
Electronic: 0974-5645

Radiative MHD Casson Non-Newtonian Nanofluid Slip Flow Induced by Stretching Cylinder: A Numerical Approach

Khyati Dang[1], Vinita Makkar[1]*, Naresh Sharma[1]*

1 Department of Basic and Applied Sciences, School of Engineering and Sciences, GD Goenka University, Gurgaon, 122103, Haryana, India

Abstract

Objectives: This article investigates the continuous magnetohydrodynamics slip flow across an extending cylinder, including heat radiation and free stream velocity. The proposed model incorporated the Brownian motion parameter and thermophoresis. **Methods:** Applying the similarity transformation to a system of partial differential equations yields an ordinary differential equation of first order. Since, there is the nonlinear nature of the modified equations, these ordinary differential equations are addressed by employing mathematical modeling. The shooting process has been embraced to solve changed equations by implementing the following Runge-Kutta Fehlberg method. **Findings:** Graphical representations are used to show how several fluid factors, such as Casson fluid parameter, free stream velocity, thermophoresis, magnetic parameter, Brownian motion parameter, heat generation parameter, Lewis number, radiation parameter, chemical reaction and curvature parameter affect concentration, temperature and velocity. Results for physical quantity of interest are also computed and reported in tabular form. The study's main findings showed that nanoparticle temperatures rise with greater Brownian motion parameter values, whereas nanoparticle concentration falls with higher heat radiation parameter values. Additionally, it is found that with rise in Lewis number rises as 0.1, 0.4, 0.7, 1.0, 1.3, heat transfer rate falls down by 21.19%. The outcomes are calculated using the MATLAB software. **Novelty:** This technique's validity is defended by comparing its most recent findings to previously published results and successfully meeting the convergence criteria. The present work emphasizes the analysis of free stream flow in the cylindrical area, specifically in the existence of partial slip and heat radiation, under convective circumstances. This study has significant implications for electronic devices such as processors as well as many businesses and the field of biological and medical sciences. The present investigation aims to support production businesses in achieving the desired level of quality of their products by effectively managing the transport phenomena.

Keywords: Stretching cylinder; Heat radiation; Brownian motion; Thermophoresis; Non-Newtonian nanofluid; Shooting technique

1 Introduction

The radiative properties of fluids are successfully increased by nanoparticles, which improves the effectiveness of heat-oriented authorities' intake. Due to its specific design purposes, the movement of warmth after heat radiation is significant. To lower the cost of manufacturing and operating nano-devices, pharmaceuticals, micro-electronics, and power modules, energy-efficient warm transit fluids are needed. The homogenous consolidation of a base liquid and nanoparticles is known as a nanofluid. Common base liquids used included oil, ethylene, and warm conductivity water. Choi and Eastman[1] came up with the idea of a "nanofluid" first. As a result, by acknowledging the impact of diffusion coefficients, Buongiorno[2] provided an explanation for the enhanced representation of nanofluid convection. By exploiting Buongiorno's model, Makkar et al.[3] examined towards the convective free-stream nanofluid's chemically reactive magnetohydrodynamic radiative flow through a stretching cylinder. In the context of magnetic and electrical forces, Jalili et al.[4] analyzed a system that rotates via a micro-polar nanofluid inserted between two parallel plates. Under the influence of a combined convection and an applied magnetic field, Kazmi et al.[5] examined the thermophysical characteristics of a mixed nanoliquid housed in a square lid driven container.

The nature of MHD conditions revolves around some of its design and exploration applications, such as cooling reactors, paper production, oil production, glass production, power generation, plasma examinations, and so forth. Seismic tremors are also increased by the research of the evolution of MHD liquid. As of late investigation of attractive field assume an indispensable part in modern and assembling processes, such as in power generator, reactor cooling and furthermore supportive in seismic tremor suspicion. MHD utilized in medication i.e., growth or disease treatment. Using a three-dimensional stretching sheet and Magnetohydrodynamic flow, V. Makkar and P. Batra[6] studied non-Newtonian nanofluids with outer velocity. Impact of MHD movement of nanofluid on an extending cylinder in the context of chemically reactive substances has been studied by V. Poply and R. Devi[7]. Heat-mass transport on micro polar fluids in MHD due to permeable and continually stretching sheet and slip phenomena generated in a porous material has been investigated via Sharma et al.[8]. In an existence of gyrotactic swimming microorganisms, Hussain and Malik[9] examined the MHD motion of nanofluid through an elongated surface. A wide variety of slip conditions, including convective boundaries and Nield conditions, are taken into account. In their study, Sarala et al.[10] examined how radiation and Hall effects influenced the MHD nanofluid motion of a vertical plate that oscillates. Nanofluid flow involving higher-order chemical reactions has been identified by Jagadha et al.[11] at three-dimensional stagnation sites. Because of a non-linear stretching sheet that generates heat, Salahuddin et al.[12] examined the internal resistance between fluid particles in tangent hyperbolic fluid flow. Khan et al.[13] discussed the zero normal flux condition, chemical interactions, and temperature and concentration dispersion of magneto-hydrodynamic Carreau fluid movement caused by an extended cylinder. Malik et al.[14] examined how magnetic field and varied thermal conductivity affect the Sisko liquid system. Salahuddin et al.[15] investigated the numerical solution of the MHD motion of hyperbolic tangent fluid through an extended cylinder with varying thermal conductivity. Hussain et al.[16] studied the magnetohydrodynamic Sisko flow of fluid through an extended cylinder in the presence of nanoparticles, taking into account the combined effects of viscous dissipation and Joule heating. Rehman et al.[17] investigated the unique properties of magnetohydrodynamic (MHD) Prandtl-Eyring nanofluid on a stretched surface.

Non-Newtonian liquids have gotten critical consideration as a result of their wide scope of utilizations in various enterprises, for instance, the construction of solid grid heat, nuclear waste exchange, engineered synergist reactors, etc. The examination of non-Newtonian liquids has made an impressive consideration because of their escalated mechanical and designing applications. Casson[18] pioneered the Casson liquid model in 1959 to visualize the color oil interlude stream. Through the production of entropy, Shah et al.[19] examined electromagnetic MHD movement of Casson nanofluid involving the energy of activation and chemical processes on a surface that is stretched exponentially. Under the impact of slip velocity in a rotating frame, Veera Krishna et al.[20] studied the radiative unsteady motion of the MHD of an incompressible viscous electrically conducting non-Newtonian Casson nanofluid mixture across a vast exponentially accelerated vertical moving permeable surface. The MHD Squeezed Radiative Movement of Casson Mixed Nanofluid Among Parallel Plates using Joule Heating has been investigated by Bhaskar et al.[21]. The numerical evaluation of the MHD thermo-mass movement of Casson ternary nanofluid combinations over an exponentially expanding cylinder has been examined by Paul et al.[22]. Akinshilo et al.[23] looked at the impact of internal heat generation by examining the nonlinear influence of heat radiation on the Casson nanofluid incorporated into a medium with pores operating over a fine needle. A stable heat flux situation with viscous heating has been examined by Kouz and Owhaib[24] in the context of a 3D rotating Casson fluid movement across an extended flat framework. The flow and heat transfer generated through a permeable stretched sheet in the context of thermal energy and an uneven heat source/sink for Casson nanofluids has been studied numerically by Bharat et al.[25]. Due to an unstable stretching sheet with radiation effect and the slip velocity occurrences, Alali and Megahed[26] studied the MHD dissipative Casson nanofluid liquid sheet movement. Using a stretching/shrinking sheet with heat radiation, Mahabaleshwar et al.[27] investigated the MHD slip flow of a Casson nanofluid mixture. In the context of Hall current, thermal rays, Brownian motion and thermophoresis, and a heat source and sink, Suresh et al.[28] examined the flow, heat, and transfer of mass characteristics of a Casson nanofluid through an exponentially extending surface. By using the Keller Box Method, Salahuddin et al.[29] examined the Mixed Convection Boundary Layer Movement of Williamson Liquid with Slip Conditions Across an Extending Cylinder. Kazmi et al.[30] used a non-Newtonian Ellis fluid model to simulate the peristaltic flow of nanofluid in a curved conduit with compliant walls.

Motivated by the already existing literature, we are therefore, expecting to unfurl the meaning of two-dimensional incompressible magnetohydrodynamics nanofluid movement caused by stretched surface in appearance of free stream velocity and heat radiation by following Buongiorno's model. No similar effort has been made before, according to a survey of recently published articles, but the current work's prosperity of thought-provoking ideas and clarity on the unusual are likely to inspire the extremely valuable interaction among disciplines. The data presented here, the authors claim, have not been reported elsewhere and may help fill any gaps. The numerical troubles showing up in the nanofluid conditions drove us to utilize the mathematical methodology. Approaching the differential framework with a Runge-Kutta-Fehlberg method will serve as the guiding concept. Practices of emerging factors on concentration, velocity and distributions of temperature are deciphered visually and in the tabular form.

2 Methodology

Two-dimensional incompressible magnetohydrodynamics nanofluid flow induced by stretched area has been taken into consideration in the current investigation, as depicted in Figure 1. The model proposed by Buongiorno encompasses the principles of Brownian motion and thermophoresis. This flow is caused by the cylinder's nonlinear nature, and the cylinder undergoes elongation with stretching velocity of $u_w = cx/L$, where c, x and Lstand for a constant, the coordinate of the surface expansion, and the length of the characteristic, respectively.

The following are modeled equations[2,7,31]

$$\frac{\partial}{\partial x}(ru)+\frac{\partial}{\partial r}(rv)=0, \tag{1}$$

$$u\frac{\partial u}{\partial x}+v\frac{\partial u}{\partial r}=\nu\left(1+\frac{1}{\beta}\right)\left(\frac{\partial^2 u}{\partial r^2}+\frac{1}{r}\frac{\partial u}{\partial r}\right)-\sigma^* B_0^2(u-U)+U\frac{\partial U}{\partial x}, \tag{2}$$

$$u\frac{\partial T}{\partial x}+v\frac{\partial T}{\partial r}=\alpha\left(\frac{\partial^2 T}{\partial r^2}+\frac{1}{r}\frac{\partial T}{\partial r}\right)+\tau\left[D_B\frac{\partial C}{\partial r}\frac{\partial T}{\partial r}+\frac{D_T}{T_\infty}\left(\frac{\partial T}{\partial r}\right)^2\right]+\frac{Q_0}{(\rho c)_f}(T-T_\infty)-\frac{1}{(\rho c)_f}\frac{1}{r}\frac{\partial}{\partial r}(rq_r), \tag{3}$$

$$u\frac{\partial C}{\partial x}+v\frac{\partial C}{\partial r}=D_B\left(\frac{\partial^2 C}{\partial r^2}+\frac{\partial C}{\partial r}\right)+\frac{D_T}{T_\infty}\left(\frac{\partial^2 T}{\partial r^2}+\frac{1}{r}\frac{\partial T}{\partial r}\right)-K_r(C-C_\infty). \tag{4}$$

Boundary conditions are:

$$u = eu_w(x) + N\mu\left(\frac{\partial u}{\partial r}\right), v = 0, T = T_w, C = C_w atr = R,$$
$$u \to U = \frac{bx}{L}, T \to T_\infty, C \to C_\infty asr \to \infty. \tag{5}$$

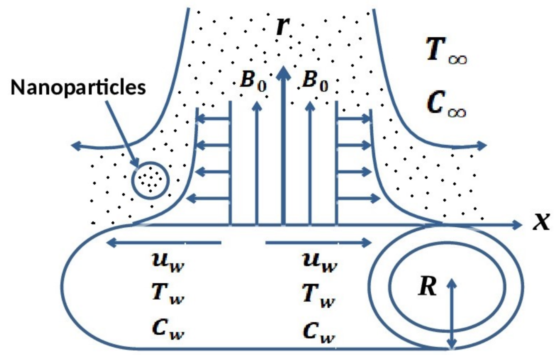

Fig 1. Physical model of the problem

Similarity transformation [31]

$$\eta = \frac{r^2 - R^2}{2R}\sqrt{\frac{c}{\nu L}}, \psi = \sqrt{\frac{\nu c}{L}} xRf(\eta), \theta = \frac{T - T_\infty}{T_w - T_\infty} \& \phi = \frac{C - C_\infty}{C_w - C_\infty}. \tag{6}$$

Transformed equations are:

$$\left(1 + \frac{1}{\beta}\right)\left[(1 + 2\eta\gamma) f''' + 2\gamma f''\right] + ff'' - f'^2 - M\left(f' - \lambda\right) + \lambda^2 = 0, \tag{7}$$

$$(1 + 2\eta\gamma)\left(1 + \frac{4}{3}Rd\right)\theta'' + \left[2\gamma\left(1 + \frac{4}{3}Rd\right) + Prf\right]\theta' + Pr\left[Nb(1 + 2\eta\gamma)\theta'\phi' + Nt(1 + 2\eta\gamma)\theta'^2 + Q\theta\right] = 0, \tag{8}$$

$$(1 + 2\eta\gamma)\phi'' + LePrf\phi' + 2\gamma\phi' + (1 + 2\eta\gamma)\frac{Nt}{Nb}\theta'' + 2\gamma\frac{Nt}{Nb}\theta' - LePrA\phi = 0. \tag{9}$$

Conditions of the final boundary follows:

$$f(0) = 0, f'(0) = e + \sigma f''(0), \theta(0) = 1, \phi(0) = 1,$$

$$f'(\eta) \to \lambda, \theta(\eta) \to 0, \phi(\eta) \to 0 asn \to \infty. \tag{10}$$

where e is the parameter for stretching/shrinking

These are some of the fluid parameters:

$$\lambda = \frac{b}{c}, Pr = \frac{\nu}{\alpha}, Sc = \frac{\nu}{D_B}, Nb = \frac{(\rho c)_P D_B (C_w - C_\infty)}{(\rho c)_f \nu}, Rd = \frac{4\sigma^* T_\infty^3}{kk^*},$$

$$Nt = \frac{(\rho c)_P D_T (T_w - T_\infty)}{(\rho c)_f T_\infty \nu}, \sigma = N\mu\frac{r}{R}\sqrt{\frac{c}{\nu L}}, M = \frac{\sigma B_0^2 L}{\rho c}. \tag{11}$$

where the parameter λ represents the free stream velocity, Sc for Schmidt number, Nb represents the Brownian motion, Rd shows the radiation parameter, Nt for thermophoresis, σ shows the velocity slip, Pr represents the Prandtl number and M for magnetic parameter.

Cf_x, Nu_x and Sh_x are defined as

$$Cf_x = \frac{\tau_w}{\rho U_\infty^2}, Nu_x = \frac{xq_w}{k\left(T_f - T_\infty\right)}, Sh_x = \frac{xq_m}{D_B\left(C_w - C_\infty\right)}. \tag{12}$$

where τ_w, q_w and q_m are defined as

$$\tau_w = \mu\left(\frac{\partial u}{\partial r}\right)_{r=R}, q_w = -\left(\alpha + \frac{16\sigma^* T_\infty^3}{3(\rho c)_f k^*}\right)\left(\frac{\partial T}{\partial r}\right)_{r=R}, q_m = -D_B\left(\frac{\partial C}{\partial r}\right)_{r=R}. \tag{13}$$

Reduced Sh_x, Cf_x and Nu_x are

$$Sh_x Re_x^{-1/2} = -\phi'(0), Cf_x Re_x^{1/2} = f''(0), Nu_x Re_x^{-1/2} = -\left(1 + \frac{4}{3}R\right)\theta'(0). \tag{14}$$

The local Reynolds number is denoted here by the equation $Re_x = U_\infty x/v$.

Numerical Scheme:

Numerical solutions are obtained by setting the step size to 0.01 and the maximum value to 10. The fact that the Shooting approach exhibits a fifth-order truncation error gives it a significant edge over other numerical strategies. Additionally, as compared to other numerical techniques, the computation of the solution is simpler. The well-known programme MATLAB is used in the current analysis to do computations using the ODE45 solver. A system of 1st order differential equations has been created using the linked differential Equation (8) through Equation (10). Shooting approach is employed to solve Equations (8), (9) and (10) and boundary conditions 11 (Equation (11)), as displayed in a flowchart in Figure 2.

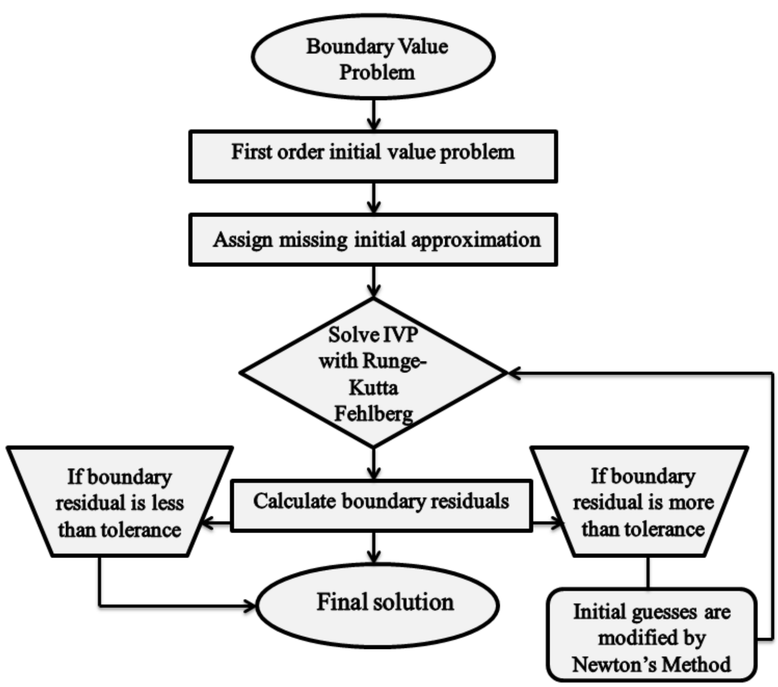

Fig 2. Flow chart of shooting procedure

The controlling ordinary differential equations are reconfigured as follows for this purpose:

$$f^{'''}=-\frac{1}{(1+2\eta\gamma)\left(1+\frac{1}{\beta}\right)}\left[\left(1+\frac{1}{\beta}\right)\left(2\gamma f^{''}\right)+ff^{''}-f^{'2}-M\left(f^{'}-\lambda\right)+\lambda^{2}\right], \tag{15}$$

$$\theta^{''}=-\frac{1}{(1+2\eta\gamma)\left(1+\frac{4}{3}Rd\right)}\left[\left[2\gamma\left(1+\frac{4}{3}Rd\right)+Prf\right]\theta^{'}+Pr\left[Nb(1+2\eta\gamma)\theta^{'}\phi^{'}+Nt(1+2\eta\gamma)\theta^{'2}+\phi\theta\right]\right], \tag{16}$$

$$\phi^{''}=-\frac{1}{2\eta\gamma}\left[LePrf\phi^{'}+2\gamma\phi^{'}+(1+2\eta\gamma)\frac{Nt}{Nb}\theta^{''}+2\gamma\frac{Nt}{Nb}\theta^{'}-LePrA\phi\right]. \tag{17}$$

A new class of variables is introduced below to help with the conversion of the previously established eqs into first-order ODEs:

$$f=\zeta(1),f^{'}=\zeta(2),f^{''}=\zeta(3),f^{'''}=\zeta(3)^{'},\theta=\zeta(4),\theta^{'}=\zeta(5),\theta^{''}=\zeta(5)^{'},\phi=\zeta(6),\phi^{'}=\zeta(7),\phi^{''}=\zeta(7)^{'}. \tag{18}$$

Equation (16) through Equation (18) are changed into the following system of D.E's in addition to Equation (19):

$$\zeta(1)^{'}=\zeta(2), \tag{19}$$

$$\zeta(2)^{'}=\zeta(3), \tag{20}$$

$$\zeta(3)^{'}=-\frac{1}{(1+2\eta\gamma)\left(1+\frac{1}{\beta}\right)}\left[\left(1+\frac{1}{\beta}\right)(2\gamma\zeta(3))+\zeta(1)\zeta(3)-\zeta(2)^{2}-M(\zeta(2)-\lambda)+\lambda^{2}\right], \tag{21}$$

$$\zeta(4)^{'}=\zeta(5), \tag{22}$$

$$\begin{aligned}\zeta(5)^{'}=&-\frac{1}{(1+2\eta\gamma)\left(1+\frac{4}{3}Rd\right)},\left[\left[2\gamma\left(1+\frac{4}{3}Rd\right)+Pr\zeta(1)\right]\zeta(5)\right.\\&\left.+Pr\left[Nb(1+2\eta\gamma)\zeta(5)\zeta(7)+Nt(1+2\eta\gamma)\zeta(5)^{2}+\zeta(6)\zeta(4)\right]\right]\end{aligned} \tag{23}$$

$$\zeta(6)^{'}=\zeta(7), \tag{24}$$

$$\zeta(7)^{'}=-\frac{1}{1+2\eta\gamma}\left[LePr\zeta(1)\zeta(7)+2\gamma\zeta(7)+(1+2\eta\gamma)\frac{Nt}{Nb}\zeta(5)^{'}+2\gamma\frac{Nt}{Nb}\zeta(5)-LePrA\zeta(6)\right], \tag{25}$$

Reduced boundary conditions are:

$$\begin{aligned}&\zeta(1)=0,\zeta(2)=1,\zeta(4)=1,\zeta(6)=1\ at\ \eta=0,\\&and\ \zeta(2)=0,\zeta(6)=0,\zeta(4)=0\ as\ \eta\to\infty.\end{aligned} \tag{26}$$

Comparison of Results:

The numerical technique is employed in order to address the physical problem by allowing for the selection of suitable values for the associated flow parameters, thereby providing flexibility for resolving the governing differential equations. Table 1 presents a contrast between our main findings for the parameter $-\theta^{'}(0)$ and significant values for the Prandtl number Pr. Comparison has been made in the absence of Brownian motion and thermophoresis parameter and for three different values of Prandtl number as 2.0, 20 and 70. Based on the findings of Kandasamy et al.[32] and Pal et al.[33], the outcomes in the current problem are well validated due to less residual error as shown in Table 1.

Table 1. Comparison of $-\theta'(0)$ for different Pr

Pr	Kandasamy et al. [33]	Residual error	Pal et al. [34]	Residual error	Present result
2.0	0.9114	0.0000	0.9113	-0.0001	0.9114
20	3.3538	0.0000	3.3539	-0.0001	3.3538
70	6.4621	-0.0001	6.4622	0.0000	6.4622

3 Results and Discussion

The fluctuations in significant fluid parameters are discussed in part of results and discussion. Graphs and tables are used to represent and provide explanations for the effects of the crucial fluid parameters. For the purposes of numerical calculations, we fixed the following values to be β =3, A =0.1,γ =0.5, λ =0.5,M =0.1, e =1, Pr =2, Q =0.1, Nb =0.3, Nt =0.3, Le =2, σ =0.1 and Rd =0.1.

Velocity distribution

The importance of the velocity profile under the impact of $\beta$is demonstrated in Figure 3**(a)**. Figure 3**(a)** illustrates how the fluid velocity increases as the size of β entry grows. This graph illustrates how raising the value of β will reduce the yield stress, which restricts fluid particle motion and reduces the thickness surface layer. Figure 3**(b)** shows the distribution of velocity against the γ. This graph demonstrated the relationship between velocity and γ . A component of the cylinder that is in touch with the fluid is shrunk when cylindrical radius decreases for larger γ, which leads to a decline in fluid resistance. As observed in Table 2, the velocity exhibits an increase while the coefficient of skin friction demonstrates a drop. Figure 3 **(c)** shows that for higher λ, the velocity gradient grows and eventually disappears nearer to the cylinder's surface. Consequently, the thermal boundary layer's diameter declines, leading to an augmentation in the outer velocity λ. The Lorentz force is identified as the principal factor responsible for the reduction in fluid velocity as depicted in Figure 3 **(d)**, is formed as an outcome of the appearance of a force field that prevents fluid particles to move freely. As a result, the momentum thickness is decreased. In order to control the final object's creation in the desired way, fluid magnetism is employed.

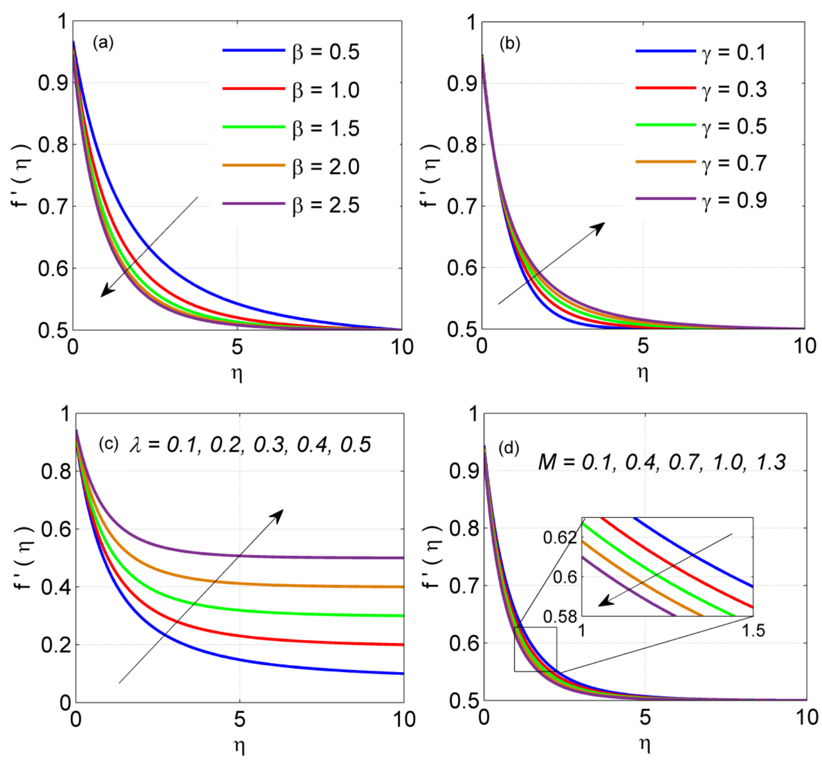

Fig 3. Velocity distribution for (a) Casson fluid parameter, (b) curvature parameter, (c) free stream velocity parameter and (d) Magnetic parameter

Table 2. Values of $f''(0)$ for distinct Casson fluid parameter β, curvature parameter γ, free stream velocity parameter λ, magnetic parameter M

β	γ	λ	M	$f''(\mathbf{0})$
0.5				-0.327948052003664
1.0				-0.428864643994954
1.5				-0.483798897149836
2.0				-0.518632319486123
2.5				-0.542754861329073
	0.1			-0.531626668732675
	0.3			-0.546473836342402
	0.5			-0.560468278050002
	0.7			-0.573738983083536
	0.9			-0.586408012132062
		0.1		-0.832951177198528
		0.2		-0.783691855734855
		0.3		-0.720882726799309
		0.4		-0.646063237316209
		0.5		-0.560468278050002
			0.1	-0.560468278050002
			0.4	-0.597058930275965
			0.7	-0.630589123381102
			1.0	-0.661619304504418
			1.3	-0.690561359236899

Temperature distribution

Figure 4**(a)** shows the temperature curve as the γ increases. Figure 4**(a)** displays the temperature rise with a boost in the curvature parameter, and Table 3 displays the corresponding rise in local Nusselt number. The growth in the local Nusselt value $Nu_x \propto -\theta'(0)$ with larger curvature parameter γ is the primary cause of the temperature increase. Figure 4**(b)** shows the impact of temperature against Lewis number and a small increment in profile is temperature observed with augmentation in Lewis number. The influence of Nb (0.5, 1.0, 1.5, 2.0, 2.5) over nanoparticle temperature distribution is depicted in Figure 4**(c)**. When liquid atoms or molecules collide, they cause Brownian motion, an arbitrary movement of those liquid particles. As a result, the thickness of surface layer increases, the nanoparticle temperature increases for greater values of Nb, and as a result, the local Nusselt number decline. Figure 4**(d)** illustrates how Ntaffects nanoparticle temperature. The temperature gradient decline as the values of the Nt rise. As a result, as seen in Figure 4**(d)**, temperature enhances as the Nt is raised. The fluctuation of the temperature profile on the heat generation parameter Q is demonstrated in Figure 4**(e)**. As stated inFigure 4**(e)**, the heat source approach allows fluids to produce heat, which extends the boundary layer and raises the temperature gradient across the fluid. Figure 4 **(f)** show the radiation parameter Rd affects field temperature. Physically, it is seen that asRdrises, the mean absorption coefficient decline. When a result, this will widen the thermal surface layer, that improves the temperature as the radiation parameter enhances, as shown in Figure 4 **(f)**.

Table 3. Values of $-\theta'(0)$ for distinct curvature parameter γ, lewis number Le, Brownian motion parameter Nb, thermophoresis parameter Nt, heat source parameter Q and heat radiation parameter Rd

γ	Le	Nb	Nt	Q	Rd	$-\theta'(\mathbf{0})$
0.1						0.468562926478968
0.3						0.508829227786408
0.5						0.548385332128601
0.7						0.587313481097714
0.9						0.625828759616194
	0.1					0.725038081492644
	0.4					0.649867681435235
	0.7					0.610833571234018
	1.0					0.587311890853752
	1.3					0.571408847785093
		0.5				0.415148163162631
		1.0				0.192489949581261

Continued on next page

Table 3 continued

1.5				0.077501820256410
2.0				0.022697836032128
2.5				-0.001353868012499
	0.1			0.648435321282220
	0.3			0.548385332128601
	0.5			0.464453405413826
	0.7			0.393967059664162
	0.9			0.334655863238195
		0.1		0.548385332128601
		0.2		0.449493375588334
		0.3		0.336243975161949
		0.4		0.201121171277604
		0.5		0.028250029479579
			0.1	0.548385332128601
			0.3	0.555905328798117
			0.5	0.555327654308700
			0.7	0.551054891146329
			0.9	0.545191339785852

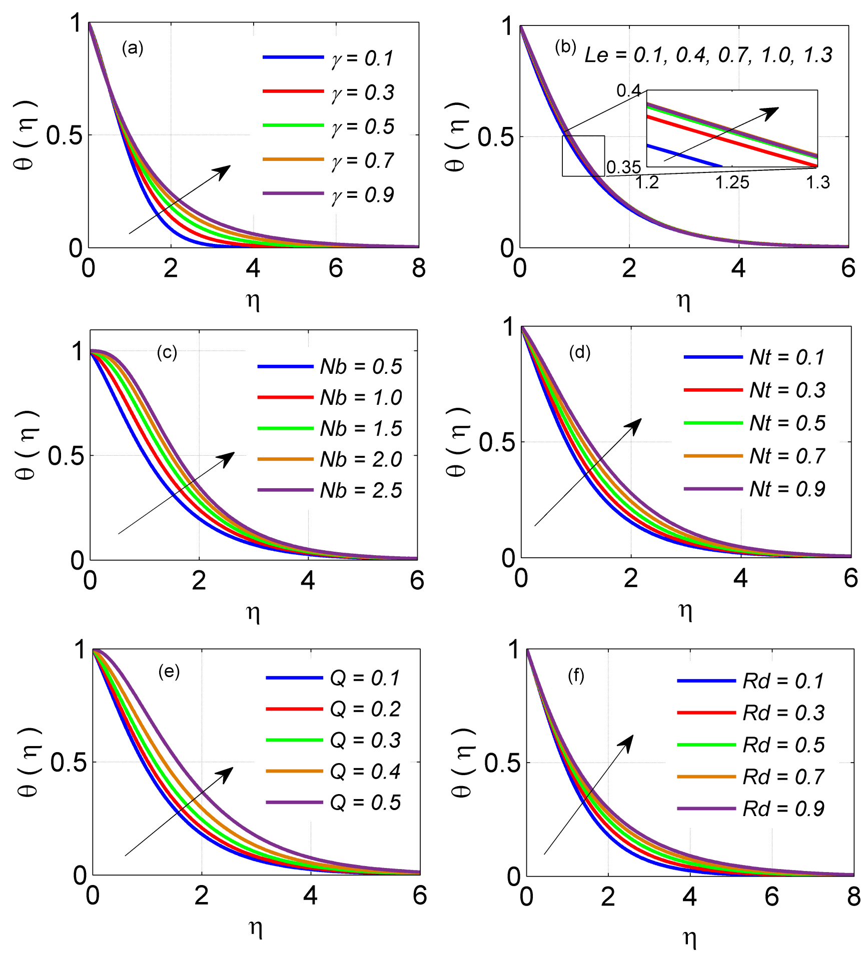

Fig 4. Temperature distribution for (a) Curvature parameter, (b) Lewis number, (c) Brownian motion parameter, (d) Thermophoresis parameter, (e) Heat source parameter and (f) Heat radiation parameter

Concentration distribution

The variation in nanoparticle concentration in relation to A is shown in Figure 5(**a**). Physically, this A aids in the consumption of species that are reactive to chemicals, which subsequently causes the volume fraction of nanoparticles to drop. As a result, concentration drops as the value of A rises, as shown in Figure 5(**a**). The concentration patterns for increasing the curvature parameter are visualized in Figure 5(**b**). Concentration rises with increasing curvature parameter, and the local Sherwood number for each increase as well, as indicated in Table 2. Figure 5(**c**) provides further visual representation of the impact of nanoparticle concentration on Nb. Here, it is seen that larger Nb contributes to a reduce in the concentration of nanoparticles. A very excellent agreement of convergence has been observed, and the concentration increases for greater Nt, as shown in Figure 5(**d**). Figure 5 (**e**) illuminates that a boost in the Prleads to a reduction in the concentration of the nanoparticles and also provides the system's nanoparticles with a sticky force. The concentration profile affected by the radiation parameter Rd has been displayed in Figure 5 (**f**) and it is recorded that concentration decline as the parameter of radiation rises.

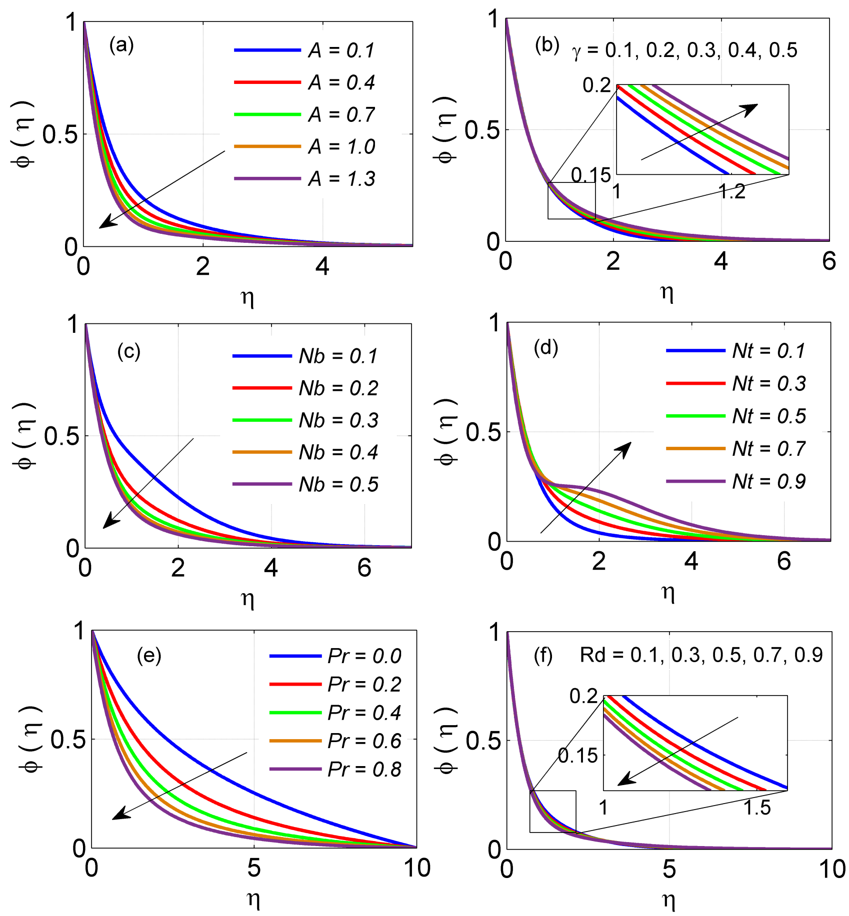

Fig 5. Concentration distribution for (a) Chemical reaction parameter, (b) curvature parameter, (c) Brownian motion parameter, (d) Thermophoresis parameter, (e) Prandtl number and (f) Heat radiation parameter

Table 4. Values of $-\theta^{'}(0)$for distinct chemical reaction parameter A, curvature parameter γ, Brownian motion parameter Nb, thermophoresis parameter Nt, Prandtl number $Pr$and heat radiation parameter Rd

A	γ	Nb	Nt	Pr	Rd	$-\theta^{'}(\mathbf{0})$
0.1						1.829964873864317
0.4						2.232493209693392
0.7						2.558725438372890
1.0						2.838111952593456

Continued on next page

Table 4 continued

1.3						3.085737686671771
	0.1					1.612638123047729
	0.2					1.668276940984085
	0.3					1.723016698529407
	0.4					1.776890099461941
	0.5					1.829964873864317
		0.1				1.575690275874324
		0.2				1.772125036793081
		0.3				1.829964873864317
		0.4				1.853584106438295
		0.5				1.863858561875853
			0.1			1.770306779029014
			0.3			1.829964873864317
			0.5			1.949910537164765
			0.7			2.108248690790149
			0.9			2.288803875703965
				0.0		0.417032406327411
				0.2		0.632024731101836
				0.4		0.810674657674036
				0.6		0.967157286805950
				0.8		1.110247612607455
					0.1	1.829964873864317
					0.3	1.804248545363635
					0.5	1.788710067595028
					0.7	1.778909222355385
					0.9	1.772543566447896

4 Conclusion

This study examines how non-Newtonian Casson nanofluids passing a stretched surface are affected by free stream velocity together with mass and heat transport. The present research in the cylindrical domain pertains to innovative free stream flow considering the effects of partial slip and heat radiation in conjunction with convective circumstances. The Shooting strategy has a substantial advantage over other numerical tactics since it displays a fifth-order truncation error. In addition, when compared to other numerical approaches, the solution calculation is easier. Similarity variables are utilized to convert PDEs in to ordinary differential equations. By using this approach, basic equations are solved. The key findings are as follows:

- Augmentation in β and$M$declines velocity distribution while velocity profile boosts for greater outer velocity and curvature parameter.
- With increase in β, skin friction coefficient declines because the Lorentz force is generated when the values of Casson fluid parameter increases.
- Temperature enhances for bigger amounts of γ, Le, Nb, Nt, QandRd.
- An increment in concentration is discovered for greater γ and Nt.
- Concentration distribution falls down for greaterA, Nb, PrandRd.

This research holds application in technological systems like semiconductors, as well as in diverse sectors and domains of biotechnology. It is difficult to hit and award an initial estimate in shooting. As a result, the procedure takes longer. This comparison may be expanded to incorporate Cattaneo-Christov heat flow, variable sheet thickness, and melting heat transfer.

References

1) Choi S, Eastman JA. Enhancing thermal conductivity of fluids with nanoparticles. *Argonne National Lab (ANL)*. 1995. Available from: https://www.osti.gov/biblio/196525.
2) Buongiorno J. Convective transport in nanofluids. *J Heat Transfer*. 2006;128:240–250. Available from: .https://doi.org/10.1115/1.2150834.
3) Makkar V, Dang K, Sharma N, Yadav S. Numerical investigation of MHD convective free stream nanofluid flow influenced by radiation and chemical reaction over stretching cylinder. *Heat Transfer*. 2022;52(3):2328–2347. Available from: https://doi.org/10.1002/htj.22786.
4) Jalili P, Narimisa H, Jalili B, Ganji DD. Micro-polar nanofluid in the presence of thermophoresis, hall currents, and Brownian motion in a rotating system. *Modern Physics Letters B*. 2023;37(01). Available from: https://dx.doi.org/10.1142/s0217984922501974.

5) Kazmi SN, Hussain A, Rehman KU, Shatanawi W. Thermal analysis of hybrid nanoliquid contains iron-oxide (Fe3O4) and copper (Cu) nanoparticles in an enclosure. *Alexandria EngineeringJournal*. 2024;101:176–185. Available from: .https://doi.org/10.1016/j.aej.2024.05.098.
6) Makkar V, Batra P. Three dimensional modeling of non-Newtonian nanofluid flow in presence of free stream velocity induced by stretching surface. *Materials Today: Proceedings*. 2022;63:283–288. Available from: https://dx.doi.org/10.1016/j.matpr.2022.03.082.
7) Poply V, Devi R. A two-component modeling for free stream velocity in magnetohydrodynamic nanofluid flow with radiation and chemical reaction over a stretching cylinder. *Heat Transfer*. 2021;50(4):3603–3619. Available from: https://dx.doi.org/10.1002/htj.22043.
8) Sharma S, Dadheech A, Parmar A, Arora J, Saranya AMQ, S. MHD micro polar fluid flow over a stretching surface with melting and slip effect. *Scientific Reports*. 2023;13(1):10715–10715. Available from: https://doi.org/10.1038/s41598-023-36988-3.
9) Hussain A, Malik MY. MHD nanofluid flow over stretching cylinder with convective boundary conditions and Nield conditions in the presence of gyrotactic swimming microorganism: A biomathematical model. *International Communications in Heat and Mass Transfer*. 2021;126. Available from: https://doi.org/10.1016/j.icheatmasstransfer.2021.105425.
10) Sarala S, Geetha E, Nirmala M. Numerical investigation of heat transfer & hall effects on MHD nanofluid flow past over an oscillating plate with radiation. *Journal of Thermal Engineering*. 2021;8(6):757–771. Available from: https://doi.org/10.18186/thermal.1201859.
11) Jagadha S, Gopal D, Kumar PV, Kishan N, Durgaprasad P. Three dimensional MHD nanoluid stagnation point low withhigher order chemical reaction. *Journal of Thermal Engineering*. 2022;8(2):286–298. Available from: https://doi.org/10.18186/thermal.1086264.
12) Salahuddin T, Khan I, Malik MY, Khan M, Hussain A, Awais M. Internal friction between fluid particles of MHD tangent hyperbolic fluid with heat generation: Using coefficients improved by Cash and Karp. *The European Physical Journal Plus*. 2017;132:1–10. Available from: https://doi.org/10.1140/epjp/i2017-11477-9.
13) Khan M, Shahid A, Salahuddin T, Malik MY, Hussain A. Analysis of two-dimensional Carreau fluid flow due to normal surface condition: A generalizedFourier's and Fick's laws. *Physica A: Statistical Mechanics and its Applications*. 2020;540. Available from: https://doi.org/10.1016/j.physa.2019.123024.
14) Malik MY, Hussain A, Salahuddin T, Awais M, Bilal S. Magnetohydrodynamic flow of Sisko fluid over a stretching cylinder with variable thermal conductivity: A numerical study. *AIP Advances*. 2016;6(2). Available from: https://dx.doi.org/10.1063/1.4942476.
15) Salahuddin T, Malik MY, Hussain A, Bilal S, Awais M. Combined effects of variable thermal conductivity and MHD flow on pseudoplastic fluid over a stretching cylinder by using Keller box method. *Inf Sci Lett*. 2016;5(2). Available from: https://www.naturalspublishing.com/files/published/692555u55j555f.pdf.
16) Hussain A, Malik MY, Salahuddin T, Bilal S, Awais M. Combined effects of viscous dissipation and Joule heating on MHD Sisko nanofluid over a stretching cylinder. *Journal of Molecular Liquids*. 2017;231:341–352. Available from: https://dx.doi.org/10.1016/j.molliq.2017.02.030.
17) Rehman KU, Awais M, Hussain A, Kousar N, Malik MY. Mathematical analysis on MHD Prandtl-Eyring nanofluid new mass flux conditions. *Mathematical Methods in the Applied Sciences*. 2019;42(1):24–38. Available from: https://doi.org/10.1002/mma.5319.
18) Casson N. Rheology of Disperse Systems. *Pergamon Press*. 1959. Available from: https://www.scirp.org/reference/referencespapers?referenceid=2717208.
19) Shah Z, Kumam P, Deebani W. Radiative MHD Casson Nanofluid Flow with Activation energy and chemical reaction over past nonlinearly stretching surface through Entropy generation. *Sci Rep*. 2020;10:4402–4402. Available from: https://doi.org/10.1038/s41598-020-61125-9.
20) Krishna MV, Ahammad N, Chamkha AJ. Radiative MHD flow of Casson hybrid nanofluid over an infinite exponentially accelerated vertical porous surface. *Case Studies in Thermal Engineering*. 2021;27. Available from: https://doi.org/10.1016/j.csite.2021.101229.
21) Bhaskar K, Sharma K, Bhaskar K. MHD Squeezed Radiative Flow of Casson Hybrid Nanofluid Between Parallel Plates with Joule Heating. *International Journal of Applied and Computational Mathematics*. 2024;10(2):80–80. Available from: https://dx.doi.org/10.1007/s40819-024-01720-w.
22) Paul A, Sarma N, Patgiri B. Numerical Assessment of MHD Thermo-mass Flow of Casson Ternary Hybrid Nanofluid Around an. *Exponentially Stretching Cylinder BioNanoSci*. 2024. Available from: https://doi.org/10.1007/s12668-024-01306-2.
23) Akinshilo AT, Mabood F, Ilegbusi AO. Heat generation and nonlinear radiation effects on MHD Casson nanofluids over a thin needle embedded in porous medium. *International Communications in Heat and Mass Transfer*. 2021;127. Available from: https://doi.org/10.1016/j.icheatmasstransfer.2021.105547.
24) Kouz WA, Owhaib W. Numerical analysis of Casson nanofluid three-dimensional flow over a rotating frame exposed to a prescribed heat flux with viscous heating. *Sci Rep*. 2022;12:4256–4256. Available from: https://doi.org/10.1038/s41598-022-08211-2.
25) Manvi BK, Kerur SB, Tawade JV, Nieto JJ, Sankeshwari SN, Ahmad H, et al. MHD Casson nanofluid boundary layer flow in presence of radiation and non-uniform heat source/sink. *Mathematical Modelling and Control*. 2023;3(3):152–167. Available from: https://dx.doi.org/10.3934/mmc.2023014.
26) Alali E, Megahed A. MHD dissipative Casson nanofluid liquid film flow due to an unsteady stretching sheet with radiation influence and slip velocity phenomenon. *Nanotechnology Reviews*. 2022;11(1):463–472. Available from: https://doi.org/10.1515/ntrev-2022-0031.
27) Mahabaleshwar US, Aly HE, Anusha T. MHD slip flow of a Casson hybrid nanofluid over a stretching/shrinking sheet with thermal radiation. *Chinese Journal of Physics*. 2022;80:74–106. Available from: https://doi.org/10.1016/j.cjph.2022.06.008.
28) Kumar SY, Hussain S, Raghunath K, K. Numerical analysis of magnetohydrodynamics Casson nanofluid flow with activation energy, Hall current and thermal radiation. *Sci Rep*. 2023;13:4021–4021. Available from: https://doi.org/10.1038/s41598-023-28379-5.
29) Salahuddin T, Malik MY, Hussain A, Awais M, Bilal S. Mixed Convection Boundary Layer Flow of Williamson Fluid with Slip Conditions Over a Stretching Cylinder by Using Keller Box Method. *International Journal of Nonlinear Sciences and Numerical Simulation*. 2017;18(1):9–17. Available from: https://dx.doi.org/10.1515/ijnsns-2015-0090.
30) Kazmi SN, Hussain A, Bilal S, Niazai S, Khan I. Numerical study on nanofluidic transport mechanism in Ellis flow within curved channel comprising compliant walls subjected to peristaltic activity. *AIP Advances*. 2024;14(7):14–14. Available from: https://dx.doi.org/10.1063/5.0216227.
31) Makkar V, Poply V. Impact of outer velocity on flow, heat and mass transfer of Casson nanofluid over a non-linear stretching sheet. *Journal of Thermal Engineering*. 2021;7(6):1353–1365. Available from: https://doi.org/10.18186/thermal.990615.
32) Khan MI, Tamoor M, THayat, Alsaedi A. MHD boundary layer thermal slip flow by nonlinearly stretching cylinder with suction/blowing and radiation. *Results in Physics*. 2017;7:1207–1211. Available from: https://doi.org/10.1016/j.rinp.2017.03.009.
33) Kandasamy R, Loganathan P, Arasu PP. Scaling group transformation for MHD boundary-layer flow of a nanofluid past a vertical stretching surface in the presence of suction/injection. *Nuclear Engineering and Design*. 2011;241(6):2053–2059. Available from: https://doi.org/10.1016/j.nucengdes.2011.04.011.
34) Pal D, Roy N, Vajravelu K. Effects of thermal radiation and Ohmic dissipation on MHD Casson nanofluid flow over a vertical non-linear stretching surface using scaling group transformation. *International Journal of Mechanical Sciences*. 2016;114:257–267. Available from: https://doi.org/10.1016/j.ijmecsci.2016.06.002.